

# Homogeneous shear turbulence

Bruno Eckhardt, Andreas Dietrich, Arne Jachens and Jörg Schumacher

Fachbereich Physik, Philipps-Universität Marburg, D-35032 Marburg, Germany

The addition of suitable volume forces to the Navier-Stokes equation allows to simulate flows in the presence of a homogeneous shear. Because of the explicit form of the driving the flows are accessible to rigorous mathematical treatment and to accurate quantitative modelling in their global properties. The statistics of the fluctuations provide insight into generic behaviour of non-equilibrium systems and into the persistence of anisotropies at small scales. Correlation functions can be used to identify dominant large scale dynamical processes that are relevant for most of the momentum transport across the shear. The numerical studies of homogeneous shear flows complement analytical and experimental investigations and contribute to bridging the gap between ideal homogeneous isotropic turbulence and the more realistic heterogeneous turbulence.

## 1 Introduction

The turbulent flow of a fluid is a paradigmatic example for a non-equilibrium, nonlinear, and self-organizing system. The flow has to be driven continuously to compensate the viscous friction due to shearing; the advection of the flow field by itself introduces a characteristic nonlinearity; and the flow shows a hierarchical organization of smaller whirls on top of larger ones<sup>1</sup>. It is one of the aims of turbulence theory to derive from the equations of motion the laws that govern this self-organization in space and time. Partial progress has been made for the theoretically most appealing case of homogeneous, isotropic turbulence, where we have the Karman-Horvath equation for third order moments<sup>1</sup>, a mean field theory<sup>2</sup>, and a variety of models<sup>1,3</sup>, but for the most part an analytical theory is not within reach. In the absence of such a formalism numerical simulations provide both access to the properties of the equations as well as guidance in developing intuition.

The power laws that describe the distribution of energy on the various scales quite well can be obtained by dimensional arguments, following Kolmogorov, Onsager, v. Weizsäcker, Heisenberg and Richardson<sup>1</sup>. These power laws are truncated on large scales by the forces that stir the fluid and on small scales by the onset of viscous dissipation. Therefore, one would like to study huge systems with infinitesimal viscosity in order to obtain as large a scaling range as possible. In terms of the large scale Reynolds number

$$Re = UL/\nu \quad (1)$$

formed by an external velocity scale  $U$ , an external length scale  $L$  and the viscosity of the fluid  $\nu$ , this is the limit of  $Re \rightarrow \infty$ . Phenomenological arguments show that the ratio between the externally imposed length  $L$  and the large eddy turnover time  $T = L/U$  to the smallest scales  $\eta$  and  $\tau$  that appear in the dynamics scale with Reynolds number like<sup>3</sup>

$$\eta/L \sim Re^{-3/4} \quad \tau/T \sim Re^{-1/2}. \quad (2)$$

Thus, the number of modes that are needed in order to represent a 3-d flow field increases like  $Re^{9/4}$ . Since the maximal time step in the integration is not determined by the time scale of the flow, but by stability considerations following from the spatial discretization,

the number of time steps increases like  $Re^{3/4}$ , so that the total operation count increases like  $Re^3$ ! As a consequence, the largest simulations run to date, on the Earth simulator with  $4096^3$  modes, achieve a Reynolds number of about 230.000 only, and follow the flow field for just one large scale time unit<sup>4</sup>. However, the comparison of data by Sreenivasan<sup>5</sup> suggests that already with a resolution of about  $256^3$  or  $512^3$  one can reach into the inertial range behaviour and thus begin to study the dominant statistical behaviour of turbulent flows. This then opens up the possibility to study flows more realistic but also more complicated than homogeneous isotropic turbulence.

In contrast to the theorists ideal, realistic flows are driven by anisotropic forcings (e.g. a uni-directional winds), influenced by boundary layers (near walls) and are in many other respects far from the case of homogeneous, isotropic turbulence. A flow that is intermediate between realistic flows and the ideal cases, and that can be used to bridge the gap is turbulence with a homogeneous, linear shear profile superimposed. It mimicks the situation that one expects to find, at least locally. An investigation of such flows then allows to study the interaction between the turbulence and the shear, the range over which the anisotropies affect the scaling behaviour, and the consequences of the shear for dynamical transport processes in the flow.

The problem with homogeneous shear flows is that it is not obvious how to maintain the shear. Driving the fluid from the boundaries, e.g. by oppositely moving side walls, will produce the familiar boundary layers with large gradients and a bulk region with reduced ones. Rogallo<sup>6</sup> thus suggested to drive the fluid by continuously shearing the computational grid. Obviously, after a while, the grid will be extremely distorted and a remeshing will be necessary in order to restore the initial resolution. When the appropriate terms are introduced into the Navier-Stokes equation, this amounts to a periodic driving of the fluid, and thus a temporally inhomogeneous situation.

In 1999 we started a research programme based on a novel method with which we can simulate homogeneous shear flows with prescribed forcing, shear, and residual turbulence. The essential idea is to employ a body force that can be tuned to fit the appropriate requirements. It is a numerical tool, not realizable in experiments, that is fairly versatile and amenable to mathematical analysis and provides insights impossible to obtain otherwise.

The outline of the article is as follows. We begin in section 2 with a description of the numerical methods used. We then turn in section 3 to a description of the global properties of the flow, the connection to rigorous mathematical bounds and to a model for the relaxation of the turbulent energy. The fluctuations around the mean properties, their probability distributions and their scaling with Reynolds number are discussed in section 4. The dynamical properties as reflected in dynamical correlation functions and their significance for large scale momentum transport are discussed in section 5. A brief outlook concludes the article.

## 2 Simulating homogeneous shear flows

The Navier-Stokes equation for an incompressible fluid driven by a divergence free volume force  $\mathbf{F}$  is, in dimensionless form,

$$\frac{\partial \mathbf{u}}{\partial t} + (\mathbf{u} \cdot \nabla) \mathbf{u} = -\nabla p + \frac{1}{Re} \nabla^2 \mathbf{u} + \mathbf{F}, \quad (3)$$

$$\nabla \cdot \mathbf{u} = 0, \quad (4)$$

with  $p(\mathbf{x}, t)$  the pressure, and  $\mathbf{u}(\mathbf{x}, t)$  the velocity field that satisfies  $\nabla \cdot \mathbf{u} = 0$ . The difficult and time-consuming part of the integration is the evaluation of the nonlinear advection term  $(\mathbf{u} \cdot \nabla)\mathbf{u}$ . High Reynolds number simulations therefore prefer Fourier representations for the velocity field, so that Fast Fourier Algorithms can be used to obtain the gradients as a local multiplication in wave number space. The aliasing problem is handled with the 2/3 rule<sup>7</sup>. In order to break the inherent periodicity of the Fourier modes, which implies that to every region with positive shear there will be one with negative shear shifted by half a period, we bound the domain by free-slip walls in the shear direction: these boundary conditions are then compatible with a Fourier representation of the velocity field.

The coordinates are chosen such that  $x$  points downstream,  $y$  in the direction of the shear, and  $z$  in spanwise direction. In  $x$  and  $z$  we take periodic boundary conditions, and in the  $y$  direction free-slip conditions, i.e.,

$$u_y = 0, \quad \text{and} \quad \frac{\partial u_x}{\partial y} = \frac{\partial u_z}{\partial y} = 0 \quad (5)$$

at top and bottom surfaces. The size of the domain is  $[0, 2\pi] \times [0, L_y] \times [0, 2\pi]$ . The length  $L_y$  is taken to be 1 or  $\pi$ . The typical Fourier resolution is  $256 \times 129 \times 256$ . As a rule of thumb the spectral resolution is considered sufficient when the largest wave number  $k_{max}$  and the smallest turbulent scales  $\eta$  satisfy  $k_{max}\eta > 1$ , although for quantities sensitive to gradients the fluctuations in  $\eta$  may have to be taken into account, so that even more restrictive conditions have to be satisfied (Schumacher and Sreenivasan, work in progress). Because of the dealiasing the largest wave number is given by  $\sqrt{2}N/3$  for  $N$  modes<sup>7</sup>.

For turbulent flows it has become customary to use not the external Reynolds number  $Re$  but an easily computable and measurable intrinsic Reynolds number  $R_\lambda = U_{rms}\lambda/\nu$ . It is based on the root mean square velocity  $U_{rms}$  and the Taylor length scale  $\lambda$  obtained from the gradients of the velocity field,

$$\lambda^{-2} = \frac{\langle (\partial u_x / \partial x)^2 \rangle}{\langle u_x^2 \rangle}. \quad (6)$$

In isotropic turbulence the relation between the large scale Reynolds number  $Re$  and the Taylor-Reynolds number  $R_\lambda$  is given by<sup>3</sup>

$$Re \approx 0.15 R_\lambda^2. \quad (7)$$

Our simulations reach up to  $R_\lambda \approx 150$  on a  $512^3$  grid for the bounded flow domains, the earth simulator<sup>4</sup> manages  $R_\lambda \approx 1200$  for isotropic turbulence.

The flow is naturally homogeneous in  $x$  and  $z$ , so that for statistical purposes we can form averages over planes  $y = const$ , henceforth denoted  $\langle \dots \rangle_A$ . It cannot be fully homogeneous in the  $y$ -direction because of the vanishing gradients at top and bottom surfaces, but the simulations show that the widths of these free slip boundary layers is small and decreases with increasing Reynolds number (see the inset of Fig. 1 and Ref. 7).

Two forms of driving are typically used: we can fix a force field  $\mathbf{F}$  and study the flow that results, or we can prescribe the mean profile and adjust the force so that this mean profile is maintained. In the latter case, the force compensates the contributions that would result from the nonlinear term and the pressure, in order to keep the amplitudes of a set of preselected Fourier components constant.

The mean profiles and the statistical properties of this flow were compared to experiment and other simulations in<sup>9</sup>. It turns out that the method easily yields a statistically

stationary state and that the dynamics of the flow is much less violent than in the case of the Rogallo remeshing, i.e. the bursts in energy and enstrophy typically found there<sup>10,11</sup> are absent.

### 3 Globally averaged properties

A quantity that is amenable to rigorous mathematics without supplementary hypothesis and additional models is the total dissipation in the mean, i.e. the turbulent dissipation averaged over the flow domain and over time,

$$\epsilon \equiv \nu \langle |\nabla \mathbf{u}|^2 \rangle_{V,T}. \quad (8)$$

The optimal bound theories of Busse<sup>12</sup>, the variational approaches of Constantin and Doring<sup>13</sup>, Kerswell<sup>14</sup> and Nicodemus et al<sup>15</sup> and their recent extension to volume driven flows<sup>16,17</sup> show that this dissipation is rigorously bounded from above by an expression of the form

$$\epsilon \leq c_1 \nu \frac{U_{rms}^2}{\ell^2} + c_2 \frac{U_{rms}^3}{\ell} \quad (9)$$

with numerical coefficients  $c_1$  and  $c_2$ . The velocity scale  $U_{rms}$  is set by the root mean square of the velocity and  $\ell$  is the length scale of the external driving. If a Reynolds number is formed with  $U_{rms}$ , i.e.  $Re = U_{rms}\ell/\nu$ , then this bound is consistent with the expectation that  $\epsilon \sim Re^3$  for large  $Re$ .

For the specific case of a sinusoidal driving the bounds and the results from a numerical simulation are shown in Fig. 1. The coefficient from the upper bound is  $c_2 = \pi^2/\sqrt{216} \approx 0.67$ , whereas the numerical simulations indicate  $c_2 \approx 0.2$ , about a factor 3 lower. It is

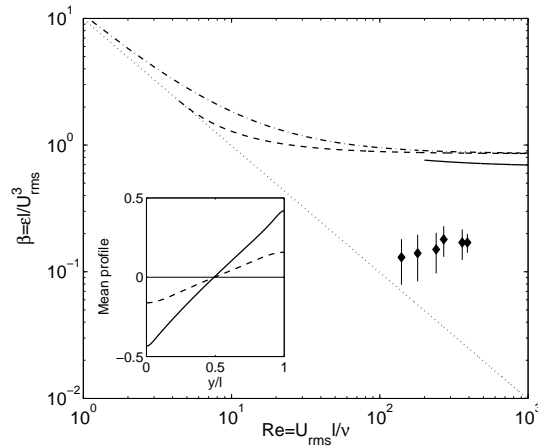


Figure 1. Dimensionless dissipation ratio,  $\beta$ , vs. Reynolds number for a flow driven by a constant shear force. The results of the direct numerical simulations are indicated by diamonds with error bars from the statistics of the fluctuations. The straight dotted line indicates lower limit to the dissipation, obtained for a laminar shear flow. The three other lines are analytically derived and successively improved bounds. The inset shows the mean flow profiles  $\langle u_x \rangle_{A,T}$  vs  $y$  for two different Reynolds numbers.

interesting to note that the difference between the bounds and the numerical simulations is much smaller than in the case of wall driven shear flows<sup>15</sup>, where the difference is about a factor 10, and that in contrast to that case the dissipation does not tend to decrease with increasing Reynolds number. This suggests that volume forces provide a more efficient stirring than moving boundaries.

The instantaneous dissipation  $\epsilon(t)$ , energy content  $E(t) = \langle \mathbf{u}^2 \rangle_V / 2$ , and energy uptake  $I(t) = \langle \mathbf{u} \cdot \mathbf{F} \rangle_V$  are not constant but fluctuate fairly irregularly. An equation for their dynamics can be derived with less mathematical rigor but still directly from the Navier-Stokes equations with minimal assumptions. Multiply the Navier-Stokes equation (3) once with  $\mathbf{u}$  and once with  $\mathbf{F}$  and average over the fluid volume. Then:

$$\frac{dE}{dt} = -\epsilon(t) + I(t), \quad (10)$$

$$\frac{dI}{dt} = -\langle \mathbf{F} \cdot [(\mathbf{u} \cdot \nabla) \mathbf{u}] \rangle_V + \nu \langle \mathbf{u} \cdot \Delta \mathbf{F} \rangle_V + \langle \mathbf{F}^2 \rangle_V. \quad (11)$$

In case the force field is an eigenfunction of the Laplacian, the term  $\langle \mathbf{u} \cdot \Delta \mathbf{F} \rangle_V$  becomes proportional to  $I(t)$ . The equations can then be closed by relating the energy dissipation and the term quadratic in the velocity in the second equation to the energy content,  $\epsilon = c_d E^{3/2}$ , and  $\langle \mathbf{F} \cdot [(\mathbf{u} \cdot \nabla) \mathbf{u}] \rangle_V = c_f E$ . Then

$$\frac{dE}{dt} = -c_d E^{3/2}(t) + I(t), \quad (12)$$

$$\frac{dI}{dt} = -c_f E(t) - \nu \lambda I(t) + F, \quad (13)$$

where the last term contains the norm of the force profile,  $F = \langle \mathbf{F}^2 \rangle_V$ . The model constants  $c_d$  and  $c_f$  can be determined from turbulent flow simulations. These equations have a stationary state, corresponding to the time average energy content and energy uptake. Interestingly, the relaxation to this stationary state is oscillatory. Fig. 2 shows a typical

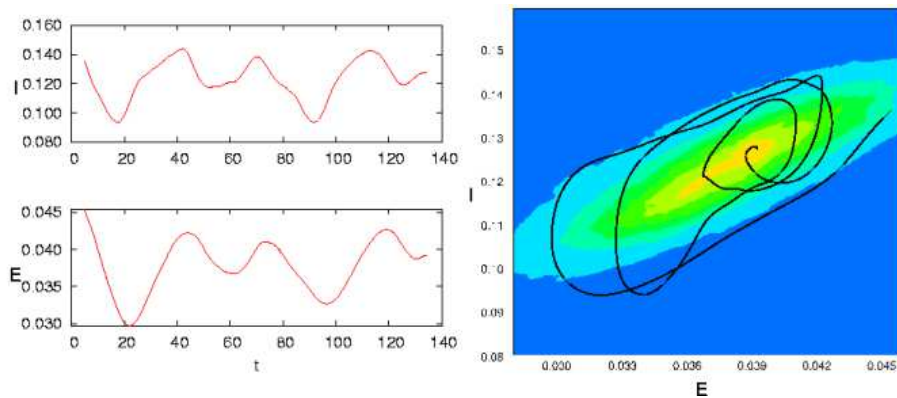


Figure 2. Comparison of the energy model with direct numerical simulations of a shear flow. The left panels show time traces of the energy content (top) and energy uptake (bottom). The panel on the right shows a typical trajectory from the DNS, superimposed on the color contours of the probability density from the model in the presence of additive white noise.

trajectory from a numerical simulation: the fluctuations that are superimposed on the mean values always drive the system away from the stationary state, but the relaxation towards the stationary state is not unlike the dynamics in the model. When the fluctuations are modelled as additive white noise the colored probability density results. The intensity of the noise was determined from the requirement that the second moments of the measured fluctuations be reproduced.

The model provides a promising starting point for the analysis of relaxational behaviour in excited turbulent flows (previously observed in<sup>18,19</sup>) and for the response dynamics of periodically driven flows<sup>20,21</sup>. In view of the exact results that could be obtained for the stationary situation it will also be interesting to see whether similar results can be obtained for periodically driven flows.

#### 4 Local fluctuations

Simulations and model in the previous section show that energy dissipation and energy uptake in a turbulent flow are fluctuating quantities, and even though they are equal in the mean, they can be different for short times. The distribution of such fluctuations is a matter of debate, with experiments by Pinton *et al.*<sup>22</sup> showing strongly non-Gaussian fluctuations, whereas the data of Cadot *et al.*<sup>23</sup> are compatible with a Gaussian distribution. Since difference may be related to the size of the domains over which the flow field was averaged we studied the local energy uptake. This also shows clear signatures for the presence of negative energy uptake, indicating a reverse flow in energy from the turbulent fluid to the stirrer. Such events are very rare, and if the average over the fluid volume is taken, they essentially never happen. However, locally the fluctuations of energy uptake rates can

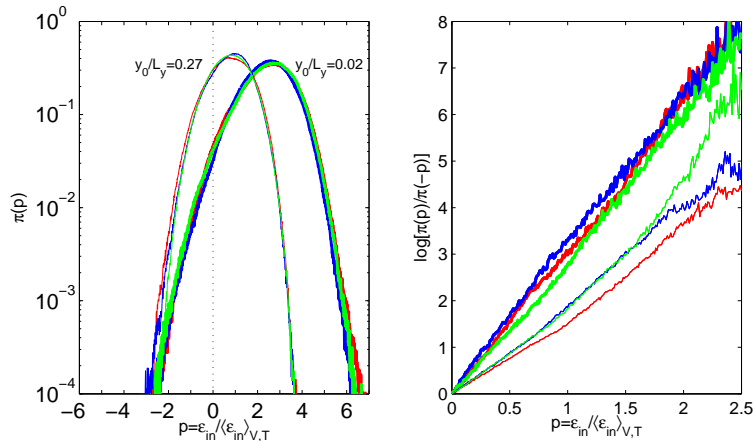


Figure 3. Statistics of energy uptake for different vertical positions in the shear layer. The probability density functions (PDF) normalized by the mean values are shown in the left panel. They are based on more than 100 turbulent snapshots separated in time by 1.5 large eddy turnover times with a total of about  $6 \times 10^8$  data points. The PDF's are shown for three different Reynolds numbers,  $Re = 270$  (red), 360 (blue) and 390 (green) and two different positions  $y_0$  in the normal direction (thin lines for 0.27 and thick lines for 0.02). The right panel shows the ratio of the probability for positive and negative energy dissipations.

take on both signs, and quite frequently become negative. Statistics of the instantaneous, pointwise energy injection rate  $\epsilon_{in}(\mathbf{x}, t) = \mathbf{u}(\mathbf{x}, t) \cdot \mathbf{F}(\mathbf{x})$  were analyzed in<sup>24</sup>. Since the system is invariant under translation in downstream and spanwise direction, but not in the normal direction, we study the distributions for planes parallel to the bounding free-slip surfaces separately. The probability density functions of the energy input rate in units of its ensemble average,  $\langle \epsilon_{in} \rangle_{V,T}$ , and for different positions between the plates are shown in Fig. 3.

The probability density functions for different Reynolds numbers collapse nicely when normalized by the mean, but the distributions vary considerably across the layer. Negative values, i.e. transfer of energy to the stirrer, occur fairly frequently, and are more likely further away from the center. The relative frequency between positive and negative energy uptake shows an exponential relation. Such exponential relations have recently been found in many non-equilibrium systems where they could be connected to fundamental symmetry properties of non-equilibrium invariant measures<sup>25</sup>. For hydrodynamic systems these ideas do not strictly apply, since the Navier-Stokes equation is not reversible. But the study of Farago<sup>26</sup> shows that even in the absence of that symmetry, as e.g. for a Brownian particle, similar relations can be justified analytically.

Since homogeneous shear flows are in a sense the first step away from ideal isotropic turbulence, one can ask how the statistical properties at the smallest scales of the turbulent flow are affected by the shear. In a pioneering paper Lumley<sup>27</sup> predicted a rapid  $R_\lambda^{-1}$  decay of such anisotropies with Reynolds number. Recent systematic measurements in simple shear flows<sup>28-31</sup> for Taylor microscale Reynolds numbers up to  $R_\lambda \sim 10^3$  show clear deviations from the predicted decay. Moreover, direct numerical simulations (DNS) for moderate Reynolds numbers confirm a persistent anisotropy and reveal a relation to typical large-scale flow structures, so-called streamwise streaks<sup>10,9,32,33</sup>. While the anisotropies still tend to become smaller with increasing Reynolds number, the decay is slower than  $R_\lambda^{-1}$ .

## 5 Dynamical correlations

Various kinds of structures in shear flows such as vortices, streaks or waves have been identified and considerable efforts have gone into identifying their dynamical origins and evolution. The isosurfaces of the downstream component of the flow field in Fig. 4 show that even though the driving is homogeneous in spanwise direction the flow organizes into large regions with very high positive (red) or negative (blue) downstream velocity. Such structures are called streaks. They induce strong gradients and shear instabilities and play an important role in a turbulent recycling process described by Waleffe<sup>34</sup> that consists of three steps: i) downstream vortices mix fluid in the normal direction and drive modulations in the downstream velocity, forming streaks; ii) streaks undergo an instability to the formation of vortices pointing in the normal direction; iii) the mean shear profile now turns these vortices again in downstream direction, thus closing the loop. Of these processes the ones in step iii) and ii) are reasonably fast, whereas the one in i) is fairly slow, since it is connected with a non-normal amplification and thus only linear in time.

The indicator for non-normal amplification that we focus on here is a temporal cross-correlation function<sup>35</sup>. Since the vortex drives the streak a cross-correlation between the vortex and the streak should be asymmetric in time: if the streak is probed after the vortex

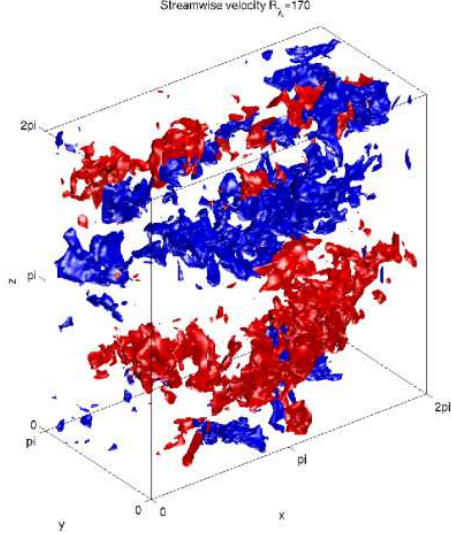


Figure 4. Isosurface plot of a turbulent streamwise velocity snapshot for a DNS of homogeneous shear turbulence at  $R_\lambda = 170$ . Level at  $v_x = 2$  is coloured red, level at  $v_x = -2$  blue. The elongated structures can be identified as streaks.

then there might be a correlation, if it is probed before then there should not be a correlation. For the fluctuations in a linearization around a linear shear profile this can be analyzed analytically<sup>35</sup>.

In order to see this in turbulent flows we study Eulerian spatial and temporal cross-correlation functions between the downstream and normal velocity components at fixed heights  $y_0$ , i.e.,

$$C_{xy}(\Delta x, \Delta t; y_0) = \langle v_y(x, y_0, z, t) v_x(x + \Delta x, y_0, z, t + \Delta t) \rangle_{x,z,t}, \quad (14)$$

The correlation function has elongated oval like isocontours that are not aligned with the axes (Fig. 5). The angle by which it is tilted gives a velocity that seems to differ a bit from the mean velocity of the flow (indicated by the green line). One-dimensional cuts, such as the one along the red line at fixed position, support an asymmetry, indicative of the non-normal amplification process<sup>36</sup>. The cut along the line given by the mean velocity (green) is what would be expected in a hot-wire anemometer at a fixed position using Taylors-hypothesis<sup>37</sup>.

## 6 Outlook

The investigations on homogeneous shear flows presented here have helped to understand the dynamics of energy and dissipation, of the behaviour of the fluctuations and the dynamical process that are active. There are several directions in which one can proceed: one option is to add tracers in order to study the dynamics in advected Lagrangian frames, especially the relative dynamics of three or more particles since it should contain information about the statistically conserved quantities in the cascade<sup>38</sup>, and since it connects to



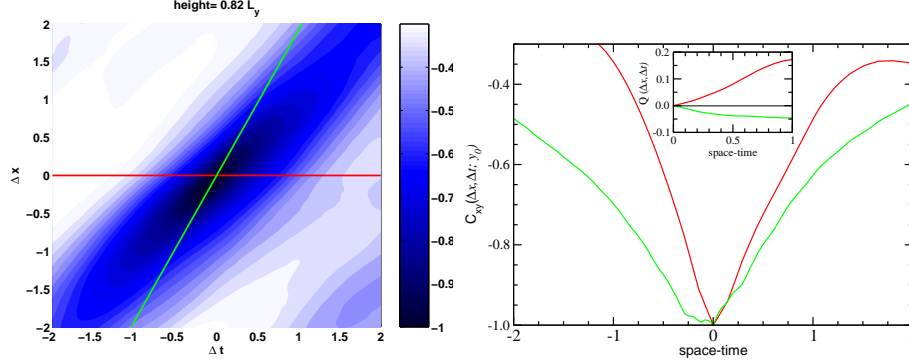


Figure 5. Spatio-temporal cross-correlation function of a turbulent shear flow evaluated at a fixed normal position  $y_0$  between the free-slip boundaries. The left panel shows the contour plots of  $C_{xy}(\Delta x, \Delta t; y_0)$  as defined in (14). The right panel shows one-dimensional cuts in time for a fixed position (red) and along a position moving with the mean velocity,  $\Delta x = \langle u_x \rangle(y_0)\Delta t$  (green). The green correlation function is one to be expected on the basis of Taylor's frozen flow hypothesis<sup>37</sup>. The inset shows the asymmetry parameter  $Q = (C(t) - C(-t))/(C(t) + C(-t))$ .

the experiments of Bodenschatz et al<sup>39</sup>. Along similar lines, it should be interesting to add scalar fields in order to study their mixing dynamics<sup>40</sup>. Active particles, like long flexible polymers, will be stretched by the flow field<sup>41</sup> and will interact with the flow and will interfere with the large scale dynamics, so as to reduce turbulent drag in the fluid. The insights gained in the homogeneous shear flow studies will be extremely valuable in understanding the properties of these added fields.

## Acknowledgements

We thank C. R. Doering, H. H. Fernholz, W. I. Goldburg, M. Oberlack, R. Pandit, W. Schröder, K. R. Sreenivasan, and P. K. Yeung for stimulating discussions. Most of the simulations were done on the Cray T90 and Cray SV1ex supercomputers at the John von Neumann-Institut für Computing at the Forschungszentrum Jülich and we are grateful for their steady support. The work was also supported by the Deutsche Forschungsgemeinschaft, by the European Network HPRN-CT-2000-00162 on Non-ideal turbulence, by the Alexander von Humboldt-Foundation within the Feodor Lynen Fellowship Program, and by Yale University.

## References

1. U. Frisch, *Turbulence*, Cambridge University Press, Cambridge 1995.
2. H. Effinger and S. Grossmann, *Z. Phys. B* **66**, 289 (1987).
3. S. B. Pope, *Turbulent flow*, Cambridge University Press, Cambridge 2000.
4. Y. Kaneda, T. Ishihara, M. Yokokawa, K. Itakura and A. Uno, *Phys. Fluids*. **15**, L21 (2003).
5. K.R. Sreenivasan, *Phys. Fluids* **27**, 1048 (1984); *Phys. Fluids* **10**, 528 (1998).

6. R. S. Rogallo, *Numerical experiments in homogeneous turbulence*, NASA Tech. Mem. 81315 (1981).
7. G.S. Patterson and S.A. Orszag, *Phys. Fluids* **14**, 2538 (1971).
8. B. Eckhardt and J. Schumacher, *Phys. Rev. E* **64**, 016314 (2001)
9. J. Schumacher and B. Eckhardt, *Europhys. Lett.* **52**, 627 (2000).
10. A. Pumir, *Phys. Fluids* **8**, 3112 (1996).
11. V. Yakhot, *Phys. Fluids* **15**, L17 (2003).
12. F. H. Busse, *Adv. Appl. Mech.* **18**, 77 (1978).
13. C.R. Doering and P. Constantin, *Phys. Rev. E* **49**, 4087 (1994).
14. R.R. Kerswell, *Physica D* **121**, 175 (1998).
15. R. Nicodemus, S. Grossmann and M. Holthaus, *Physica D* **101**, 178 (1997); *J. Fluid Mech.* **363**, 281 (1998).
16. C.R. Doering and C. Foias, *J. Fluid Mech.* **467**, 289 (2000).
17. C. R. Doering, B. Eckhardt and J. Schumacher, *J. Fluid Mech.* **494**, 275 (2003).
18. A. Schmieguel and B. Eckhardt, *Europhys. Lett.* **51**, 395 (2000).
19. J. Schumacher and B. Eckhardt, *Phys. Rev. E* **63**, 046307 (2001).
20. O. Cadot, J. H. Titon and D. Bonn, *J. Fluid Mech.* **485**, 161 (2003).
21. A. von der Heydt, S. Grossmann and D. Lohse, *Phys. Rev. E* **67**, 046308 (2003).
22. S. T. Bramwell, P. C. W. Holdsworth and J.-F. Pinton, *Nature* **396**, 552 (1998).
23. J. H. Titon and O. Cadot, *Phys. Fluids* **15**, 625 (2003).
24. J. Schumacher and B. Eckhardt, *Physica D*, in press (2003).
25. D. J. Evans, E. G. D. Cohen and G. P. Morriss, *Phys. Rev. Lett.* **71**, 2401 (1993).
26. J. Farago, *J. Stat. Phys.* **107**, 781 (2002).
27. J. L. Lumley, *Phys. Fluids* **10**, 855 (1967).
28. S. Garg and Z. Warhaft, *Phys. Fluids* **10**, 662 (1998).
29. M. Ferchichi and S. Tavoularis, *Phys. Fluids* **12**, 2942 (2000).
30. X. Shen and Z. Warhaft, *Phys. Fluids* **12**, 2976 (2000).
31. A. Staicu and W. van de Water, *Phys. Rev. Lett.* **90**, 094501 (2003).
32. J. Schumacher, *J. Fluid Mech.* **441**, 109 (2001).
33. J. Schumacher, K. R. Sreenivasan and P. K. Yeung, *Phys. Fluids* **15**, 84 (2003).
34. F. Waleffe, *Phys. Fluids* **9**, 883 (1997).
35. B. Eckhardt and R. Pandit, *Eur. J. Phys. B* **33**, 373 (2003).
36. B. Eckhardt, A. Jachens and J. Schumacher, *Reynolds number scaling in turbulent flow*, A.J. Smits (ed.) Kluwer Academic Publishers, 2003, pp. 253–256.
37. A.A. Townsend, *The structure of turbulent shear flows*, 2nd ed. (Cambridge University Press, Cambridge, 1976)
38. G. Falkovich, K. Gawedzki and M. Vergassola, *Rev. Mod. Phys.* **73**, 913 (2001).
39. A. La Porta, G. A. Voth, A. M. Crawford, J. Alexander and E. Bodenschatz, *Nature* **409**, 1017 (2001).
40. J. Schumacher and K.R. Sreenivasan, *Phys. Rev. Lett.* **91**, 174501 (2003).
41. B. Eckhardt, J. Kronjäger and J. Schumacher, *Comp. Phys. Commun.* **147**, 538 (2003).